Pedestrian Thorax Impactor Design and Biofidelity Validation

Yongcheng Long, Tao Sun, Yu Liu, Zhi Xiao, Yu Xiao, James Cheng, Guanjun Zhang

Abstract Among the serious injuries caused by pedestrian traffic accidents, the thorax has become the second most injured part after the head, and it is of great significance to carry out research on the protection of pedestrian thorax injuries. However, there are no effective assessment tools and methods for the pedestrian thorax. Based on the analysis of the epidemiology of pedestrian thoracic injuries and injury mechanisms, this study designed an anterior-posterior symmetric semi-thoracic impactor incorporating anthropomorphic ribs in accordance with human thoracic anatomical dimensions. A finite element model was established and its biofidelity was validated through lateral impact tests on the thoracic module and whole-body coupled lateral impact tests. To investigate the predictive ability of the thorax impactor's deflection, a collision matrix between a simplified vehicle model and a THUMS pedestrian was established by varying bumper height and hood angle. The thorax impactor, mounted along a guide rail with lateral rotation allowed, was directed to impact corresponding vehicle positions using the velocity of T8 (8th thoracic vertebra) along the hood normal direction at the time of maximum thoracic deflection.

In the lateral impact test of the thoracic module, the thoracic deflection measured by the thorax impactor was comparable to that of the WorldSID and fell within the response ranges of the THUMS and GHBMC human thoracic finite element models. In the whole-body coupled lateral impact test using the thorax impactor coupled with the WorldSID model, the pendulum impact force of the thorax impactor met the ISO/9790 response corridor requirements, and both the pendulum impact force and thoracic deflection aligned well with human biomechanical experimental data. In the full-vehicle collision scenario, the thoracic deflection measured by the thorax impactor also showed consistency with the THUMS-derived thoracic deflection. The findings indicate that the thorax impactor demonstrates robust biofidelity, rendering it suitable for evaluating vehicle performance in pedestrian thoracic injury mitigation.

Keyword Biofidelity, Finite element models, Pedestrian, Thorax impactor, Torso.

I. INTRODUCTION

Pedestrians, as vulnerable road users (VRUs), are directly exposed to traffic environments without personal or vehicle-based protective measures, rendering them susceptible to severe or fatal injuries in traffic accidents. Globally, approximately 1.18 million fatalities occur annually due to traffic collisions, with pedestrians accounting for 22% of these deaths [1,2] Pedestrian safety has emerged as a critical global public health challenge [3]. The implementation of assessment protocols utilising evaluation tools such as the head impactor, upper legform impactor, and lower legform impactor has improved vehicle front-end design, significantly enhancing protection for corresponding body regions. This progress has reduced head injury risks by over 80% and markedly decreased lower extremity injuries [4]. Statistical analyses of pedestrian traffic injuries reveal that 42.2% of pedestrians sustain Abbreviated Injury Scale 3+ (AIS3+) thoracic injuries, second only to head injuries (78.1%) [5]. Therefore, the development of pedestrian thoracic assessment tools will help enhance vehicle protection for pedestrians' chests.

Scholars and institutions have conducted research on pedestrian thoracic assessment tools. Reference [6] concluded through experimentation that the thorax of side-impact dummies with high biofidelity could be used to evaluate thoracic injuries in pedestrians caused by vehicles with higher hoods, such as sports utility vehicles (SUVs) . Consequently, in [7], proposed the Thorax Injury Prediction Tool (TIPT), developed using a thorax module derived from the EUROSID-2(ES-2) dummy. However, its correlation with Total Human Body Model for Safety(THUMS)-predicted thoracic injuries in real-world vehicle tests proved suboptimal. Reference [8] also designed a simplified thorax impactor, ThImp-PED, based on the ES-2 thoracic structure, and investigated its injury reproduction performance in collisions involving SUVs and light trucks (LTVs) with flat-front designs. Both ES-2-derived impactors employ rail-guided deformation mechanisms, restricting rib motion to lateral displacement. Studies by [9] demonstrated that such designs reduce thoracic deflection by approximately 22% under 20° anterior-lateral loading and 34% under 30° anterior-lateral loading compared to pure lateral loading [10]. Given that pedestrian thoracic injuries often involve combined lateral deformation and longitudinal deflection, rail-guided mechanisms may inadequately replicate real-world thoracic responses. Reference [11] highlighted that the WorldSID dummy, which utilises an inner-outer

G. Zhang (E-mail: zgjhuda@hnu.edu.cn; Tel: +86-18570327941) and Z. Xiao are Associate Professors at the State Key Laboratory of Advanced Design and Manufacturing Technology for Vehicle, Hunan University, China. Y. Long, Y. Liu and J. Cheng are Researchers at China Automotive Engineering Research Institute Co., Ltd., Chongqing, China. T. Sun and Y. Xiao are Students at Hunan University, Changsha, China.

ribcage structure to simulate human anatomy, exhibits superior biofidelity under multi-directional loading, and effectively reflects thoracic injury patterns in accident reconstructions [12].

Therefore, to develop a thoracic testing device that adapts to pedestrian thorax impact conditions while demonstrating high biofidelity, in this paper, an anteroposteriorly symmetric semi-thoracic impactor with dual-bone-ring structure is designed.

II. METHODS

Structural Design of Thorax Impactor

The design of the thorax impactor should consider its biofidelity, test repeatability, and reproducibility. Approximating human anatomical structures helps ensure biofidelity. Simplified structure will contribute to test repeatability and reproducibility.

Statistical analysis of pedestrian accidents reveals that lateral collisions account for 80% of total incidents [13], necessitating thorax impactors to prioritise replication of biomechanical responses during side impacts. In fatal pedestrian collisions, 63.3% of casualties present rib fractures as the predominant thoracic injury [14], with associated intrathoracic trauma (hemothorax, pulmonary contusions, aortic rupture) frequently co-occurring with rib fractures [15-18]. Consequently, the impactors primarily focus on predicting rib fracture risks. The WorldSID anthropomorphic test device (ATD) demonstrates effective thoracic response reproduction through its osseous-ring structure that mimics human ribcage characteristics: comparable viscoelastic properties, multi-directional deformation capacity, and validated performance in biofidelity assessments across impact vectors [10]. This informed our design choice of adopting a damped osseous-ring configuration.

Given the predominant occurrence of rib fractures on the impact side in pedestrian accidents [19], the device employs a semi-thoracic configuration that simultaneously reduces launcher system complexity and facilitates impact interface integration. Although human ribs exhibit anatomical asymmetry with non-orthogonal spinal alignment, for the convenience of processing and manufacturing, the impactor's rib plane was standardised orthogonal to the spinal axis with anteroposterior symmetry, as shown in Figure 1. To enhance calibration efficiency and component interchangeability within the rib-ring assembly, thoracic ribs were standardised with identical geometric parameters. Human anatomical studies indicate that the transverse diameter of ribs at shoulder height is smaller than that of lower ribs. Meanwhile, pedestrian traffic accident statistics show that rib fractures at shoulder level account for a relatively low proportion of thoracic injuries in collisions [20]. Therefore, the current shoulder-rib design of the thoracic impactor follows the dimensions of the WorldSID dummy's shoulder ribs.

The inertial parameters of the impactor, including its centre of mass position and moment of inertia, constitute fundamental structural characteristics. Utilising anthropometric data from the 50th percentile male population and dimensional parameters of existing ATDs, the thorax impactor's dimensions were defined as Table 1. Epidemiological statistics demonstrate that ribs 3 to 10 exhibit the highest injury probability in pedestrian accidents [21], while fractures of ribs 1 to 2 are associated with cardiopulmonary trauma and elevated mortality rates [20]. Consequently, the vertical height of the impactor (344 mm) spans from the glenohumeral joint to the inferior margin of the 10th rib to encompass these critical injury zones. In anthropometric terms, thoracic width is defined as the transverse distance between the most lateral protrusions of the ribcage at nipple-level height. For this study, the semi-thoracic width was standardised to 173 mm. Thoracic depth refers to the sagittal-plane distance between the most anterior and posterior protrusions of the torso at nipple-level height. This parameter was set to 236 mm based on validated anthropometric datasets[22]. To accurately replicate human mass distribution, the impactor's total mass (excluding mounting brackets) was designed as half of the complete thoracic mass, resulting in a target value of 11.4 kg.

TABLE I
Geometric dimensions and mass characteristics of the thorax impactor

Data sources	Width	Thickness	Height	Mass
THUMS	314	244	344	20.47
GHBMC	324	222	342	14.13
ES-2re	331	281	233	22.4±1.0
WorldSID	378	243	H1:279/H2:220	20.56±0.35
[22]	284-379/332	—	352-465/403	—
[23]	340	—	—	—
[24]	311	229	—	—
GJB 9872-2020	329	222	—	—
[25]	298	218	—	—
Thorax impactor	173(346)	236	344	11.4

The thorax impactor employs thoracic deflection as an injury criterion. Thoracic deflection serves as a critical indicator for evaluating injury risks during thorax impacts, demonstrating strong correlation with rib fracture occurrence [26], and has been extensively adopted in occupant safety evaluation protocols including frontal collisions and lateral impacts. For instance, in Euro-NCAP (Euro New Car Assessment Programme), Japan-NCAP (Japan New Car Assessment), and China-NCAP (China

New Car Assessment) lateral impact test procedures, the WorldSID 50th ATD utilises thoracic deflection as the definitive injury criterion, with established high-performance limits (28 mm) and low-performance thresholds (50 mm). Moreover, this injury criterion can be conveniently measured by relatively mature sensors such as 2D-IRTRACC.

The impactor is wrapped with foam pads and skin to simulate the biomechanical response of human skin and muscle deformation. The outer ring of the rib is firmly connected to the foam pad to simulate the muscular action between the ribs. The impactor is connected to the launching mechanism through the mounting base. A Coulomb friction torque threshold (12.43 N· m) is implemented at the mounting interface, against rotation during launch acceleration.

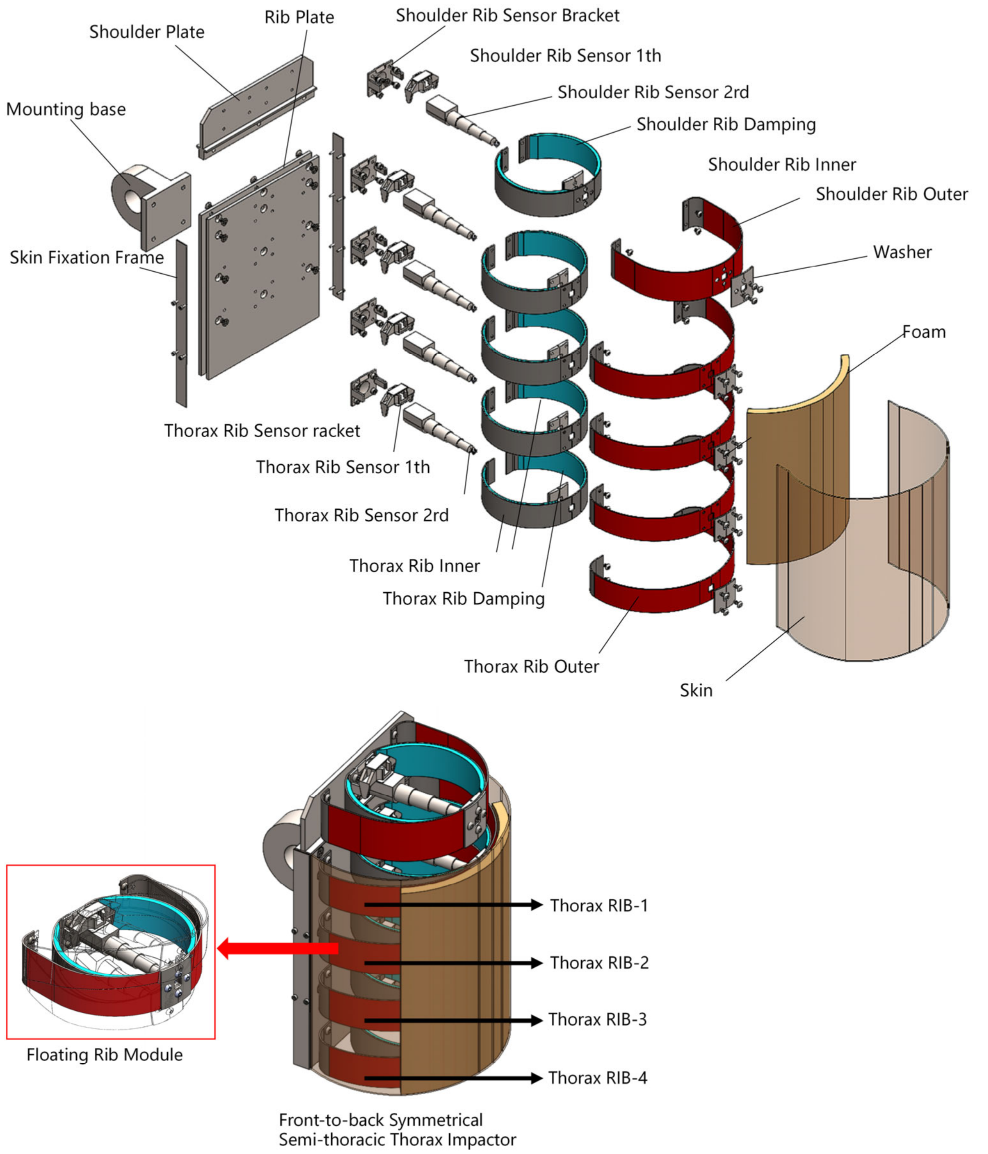

Fig. 1. Schematic diagram of thorax impactor structure.

Finite Element Modelling of the Thorax Impactor

The rib assembly employs shell elements for both inner and outer steel rings, with thicknesses of 1.1 mm and 1.15 mm, respectively, utilising #30 shape memory alloy material from LS-DYNA. Rib damping is simulated via solid elements assigned to #6 viscoelastic polymer material. Non-deformable components, including the rib plate and mounting base, are modelled as #20 rigid material to optimise computational efficiency. Rigid components are coupled using *CONSTRAINED_RIGID_BODY keywords to simplify threaded joint representation. The 2D-IRTRACC mechanism is kinematically reconstructed to replicate inertial properties, with thoracic deflection quantified via *ELEMENT_DISCRETE definitions. The static frictional torque at the mounting base interface is configured via the *CONSTRAINED_JOINT_STIFFNESS_TRANSLATION keyword to 12.43 N·m. The finite element model of the thorax impactor employs a uniform element size of 5 mm, comprising 55,448 elements and 52,813 nodes.

Biofidelity Validation

This study investigated the biofidelity of the thorax impactor through three distinct biomechanical loading scenarios: 1) thorax module lateral impact, 2) full-body coupled lateral impact, 3) thoracic module-to-hood impact.

Thorax Module Lateral Impact

The lateral pendulum impact to the thorax, serving as the standard validation scenario for the WorldSID dummy, was employed in this study to assess the thorax impactor' s deflection response characteristics. Comparative analyses were conducted against the thorax responses of the WorldSID dummy and two human body models (THUMS and Global Human Body Models Consortium (GHBMC)).

Based on anatomical demarcations between the human thorax, neck, and abdomen, the design retains components between the SPINEBOX_UPPER_BRACKET and LUMBAR_MOUNTING_WEDGE from the WorldSID, while removing bilateral upper extremities and preserving thoracic clothing/foam layers. In the human body models, spinal structures above T1 and cervical components were removed, defining the thoracic region through a horizontal plane at the inferior border of the 10th rib. A skin-simulated enclosure surface was created at the thoracoabdominal section, connected via shared nodes with thoracic skin and musculature, while establishing contact interfaces with visceral organs to maintain physiological motion. Incomplete visceral geometries from planar sectioning were geometrically repaired to ensure model stability. Musculoskeletal modifications included removal of bones and muscles distal to the glenohumeral joint, preserving scapular bones and supraspinous fossa-contained muscle units. For the THUMS model, endpoints of one-dimensional elements originally connected to the humerus were reattached to the scapula to maintain thorax muscle kinematics. Unconstrained muscle cross-sections at the shoulders and neck were fixed by rigidly connecting residual tissue nodes to the humerus and T1 vertebra.

To ensure identical pendulum impact positions across four models, postural alignment was performed as follows: 1) All models were vertically oriented; 2) T8 vertebrae of two human body models were aligned, the shoulder centre of the thorax impactor' s bracket was matched with the glenohumeral joints of human models, and the T8 accelerometer mounting position on the WorldSID thoracic module was aligned with human T8. Rib plates were fixed for the thorax impactor and WorldSID thorax module, while spinal vertebrae in human finite element models were rigidised and fully constrained in all degrees of freedom.

The 23.4 kg pendulum' s central axis was aligned with the second thoracic rib of the thorax impactor, the second thoracic rib of the WorldSID, and the outermost point of the seventh rib' s central axis in the human body models. Impacts were conducted at 4.3 m/s, with a friction coefficient of 0.3 set between the pendulum and all four models, as shown in Figure 2.

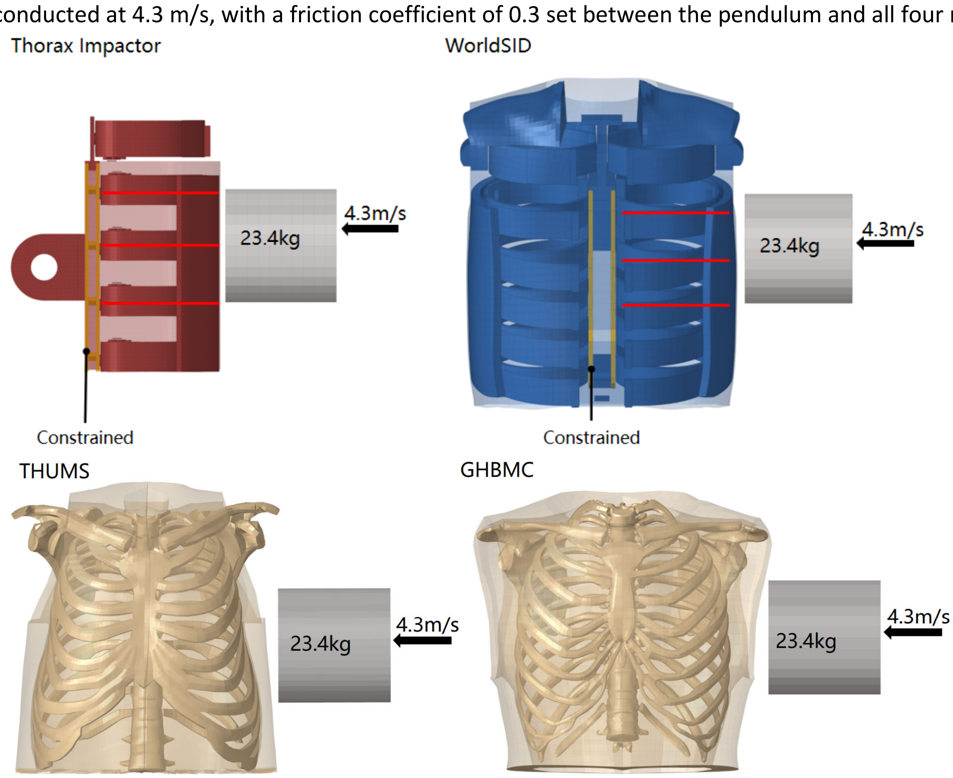

Fig. 2. Thorax module lateral impact. Rigidify the spine and constrain all degrees of freedom. The red line is semi-thoracic deflection measurement in thorax module.

A central node is defined along the transverse plane at the lateral aspect of the impacted rib's nodal array, which is rigidly constrained to the stiffened spinal column. Uniaxial discrete elements (type *ELEMENT_DISCRETE) are implemented between the lateral nodal cluster of the impacted rib and this thoracic centroid, enabling quantification of rib-specific thoracic deflection during the collision process, as schematically illustrated in Figure 3.

A corresponding thoracic centroid node is established along the transverse anatomical plane at the lateral nodal cluster of the impacted rib, which is rigidly constrained to the rigidised spine. A discrete element is created between the impacted rib's lateral nodes and this centroid node to output the deflection value, as illustrated in Figure 3.

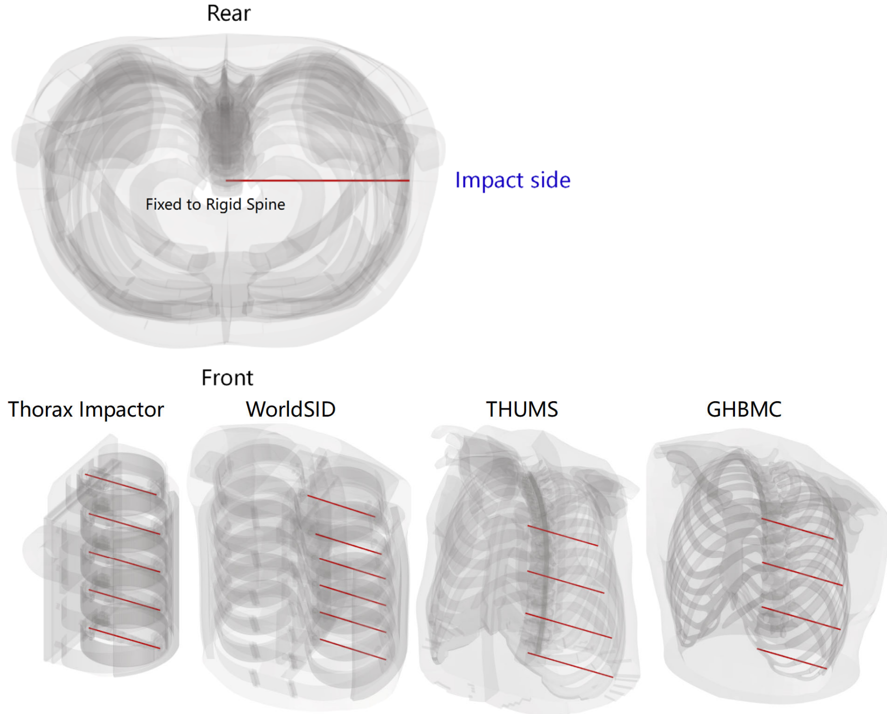

Fig. 3. Arrangement of semi-thoracic deflection measurement in thorax module lateral impact conditions.

Full-Body Coupled Lateral Impact

This study couples the thorax impactor with a whole-body WorldSID dummy model to conduct lateral thoracic impact simulations, comparing the results with post-mortem human subject (PMHS) thoracic response data to validate the biofidelity of the impactor model.

The thoracic section of the WorldSID was removed, including the spinebox sideplates, all ribs, non-impact side arm, andthe jacket, while preserving the lower neck bracket and lumbar mounting wedge, as illustrated in Figure 4(a). The thorax impactor was posture-aligned with the WorldSID according to three alignment criteria: 1) concentricity of glenohumeral rotational axes, 2) angular correspondence of vertebral column inclination, and 3) midsagittal plane co-registration, as demonstrated in Figure 4(b).

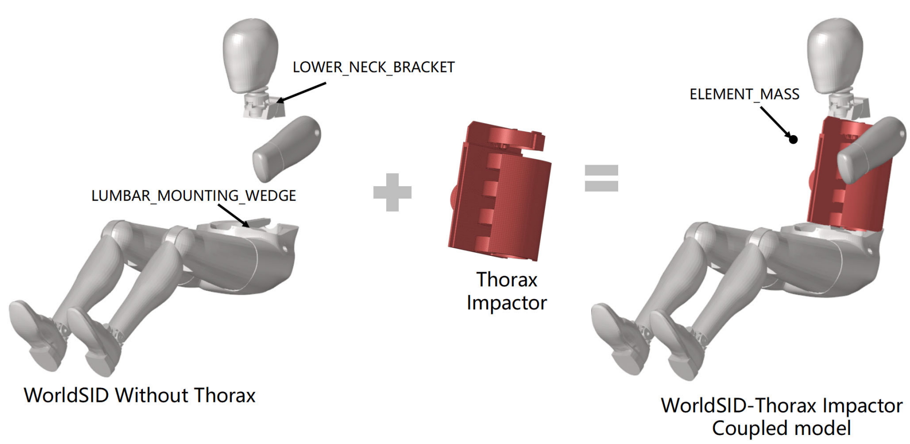

a) Schematic representation of model coupling

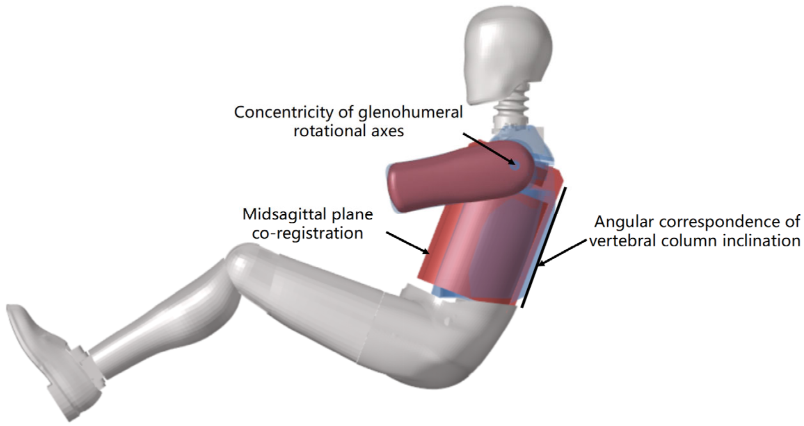

b) Thoracic pose registration benchmark

Fig. 4. Biomechanical coupling interface of thorax impactor and WorldSID dummy.

To maintain identical inertial parameters between the coupled model and the original WorldSID, a concentrated mass point was added to the thoracic region as shown in Figure 4(a). The inertial parameters of the coupled model are presented in Table Ⅱ.

TABLE II
COMPARISON OF INERTIA PARAMETERS BETWEEN COUPLED MODEL AND WORLDSID MODEL

Model	Mass/kg	Center of gravity/mm			Moment of inertia/ (t·mm²)		
		X	Y	Z	I_{XX}	I_{YY}	I_{ZZ}
Coupled model	74.26	170.13	-5.94	352.32	3866.8	9282.7	7363.8
WorldSID	74.26	169.59	-1.53	346.83	3828.4	9297.4	7365.0

The coupled model and WorldSID dummy were positioned on rigid seat fixtures with cushion and backrest inclination angles of 21° and 113°, respectively, as illustrated in Figure 5. A dynamic gravitational preloading sequence was implemented to induce prestress states, while maintaining synchronized postural alignment of the torso, pelvis, head, neck, and upper extremities across both models. The friction coefficient between the models and seating surfaces was set to 0.3. Following PMHS test protocols, a 23.4 kg pendulum was used to laterally impact the centreline of the second rib at 4.3 m/s, with the exclusion of upper limb contact interactions [27-29]. The coupling efficacy was validated by analysing displacement and acceleration data at four anatomical locations: head, thoracic vertebrae T4/T12, and pelvis.

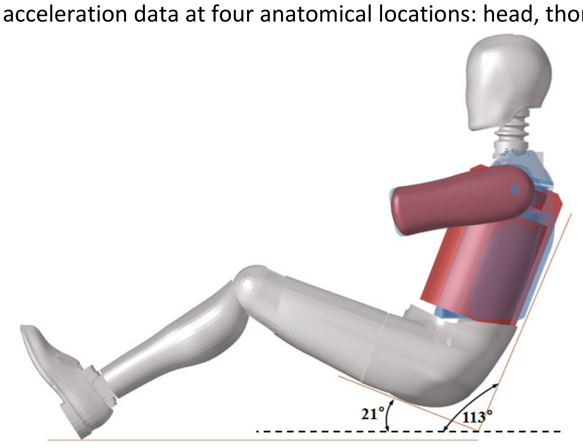

Fig. 5. Seated posture configuration of coupled model in lateral impact loading.

The thoracic deflection of the coupled model and the centroidal acceleration of the pendulum (for impact force derivation) were quantified and comparatively analyzed against PMHS experimental datasets and WorldSID test device calibration profiles to evaluate the biofidelity of the thorax impactor assembly.

Thoracic Module-to-Hood Impact

To investigate the injury prediction capability of the thorax impactor in vehicle collision conditions, numerical models were established for collisions involving the thorax impactor, the THUMS human body model, and different stylised vehicles. The relationship between the thoracic deflection measured by the impactor and the thoracic deflection of the human model was analysed. The simplified vehicle models were constructed based on Euro-NCAP pedestrian protection protocols, utilising mean external geometries derived from production vehicle contours. Structural stiffness calibration was performed in compliance with European pedestrian impact validation requirements [30]. Three different bumper lead-edge heights (BLEH): 600 mm, 800 mm, and 1000 mm and seven hood angles (ranging from 10° to 70°) were combined to generate 21 distinct vehicle configurations. The THUMS pedestrian posture was configured according to Euro-NCAP TB024 specifications, maintaining left foot forward and right foot rearward [31]. The vehicle impacted the stationary pedestrian laterally at an initial speed of 40 km/h, with a friction coefficient of 0.3 set between the vehicle and THUMS.

Given the viscoelastic compliance and multi-directional mobility of the human thorax during impact events, significant variations in velocity are observed across thoracic regions. This investigation establishes the T8 thoracic vertebra – positioned at the biomechanical centroid of the THUMS thorax segment, as the representative kinematic reference for thorax module velocity characterisation. The velocity of the T8 centre point relative to the vehicle along the hood normal direction at the moment of thoracic contact was defined as the initial launch velocity of the thorax impactor.

The impact location on the vehicle was determined as the position corresponding to the centre of the seventh rib at the moment of thoracic contact. The impactor was orthogonally aligned with the strike centroid's normal vector, subsequently launched along the surface normal direction at the predetermined initial velocity derived from THUMS kinematic analysis. The impactor was constrained to translate along a guide rail while being permitted to rotate about its mounting axis after hood contact, as illustrated in Figure 6. A friction coefficient of 0.3 was assigned between the impactor and the vehicle.

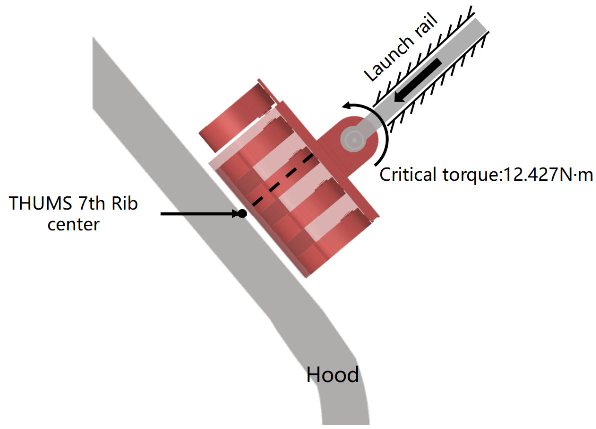

Fig. 6. Schematic diagram of thorax impactor firing method.

Since the spinal motion characteristics differ between the full-body model and the rigidified thoracic module, a semi-thoracic deflection measurement method with mobile spinal interface was adopted to quantify thoracic deflection in the human model. Through CONSTRAINED_INTERPOLATION, a dynamic reference point was established as the semi-thoracic reference point, moving synchronously with the sternum and the spine. The semi-thoracic deflection value was output via discrete elements connecting the impacted-side rib's outer nodes to this central reference point (Figure 7). Comparative analysis of thoracic deflection responses between the human body model and impactor subsystem was conducted.

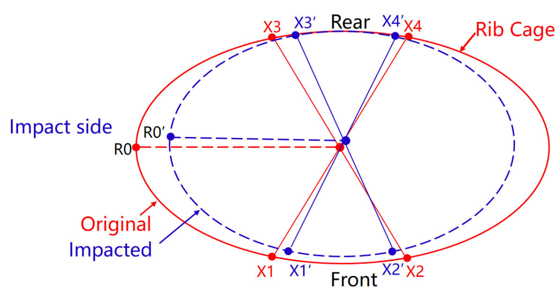

Fig. 7. Schematic diagram of semi-thoracic deflection measurement method in THUMS model.

Points X1 and X2 are located on the sternum, while points X3 and X4 are situated on the transverse processes of the vertebral body. The geometric center of these four points is defined as the semi-thoracic reference point. R0 is positioned on the rib at the lateral aspect of the body. The discrete element connecting R0 and the semi-thoracic reference point serves as the semi-thorax deflection.

Semi-thoracic deflections

The thorax impactor in this study adopted a semi-thorax structure. Consequently, the thorax deflection derived from the impactor is limited to unilateral thoracic deflection response, formally defined as semi-thoracic deflection. While in biomechanical testing of the human thorax, the compressive deformation of the entire ribcage is typically quantified, such as [23][27][28]. Therefore, to compare with the impact force-deflection responses of PMHS thorax, the fitting relationship between full-thoracic deflection and semi-thoracic deflection was established in this study.

The family car (FCR) and SUV models defined in TB024 technical bulletin [30] were used to impact THUMS pedestrian models at 40 km/h 50 km/h and 60 km/h, respectively. Three pedestrian positions relative to vehicles were defined by rotating pedestrians 30° left/right around vertical axes. Three BLEH vehicle configurations were created by lifting vehicles 50mm and 100mm. The simulation matrix containing 11 tests is presented in Table A-2. Eleven computational models are schematically depicted in Figure A-3. The full-thoracic and semi-thoracic deflection were output at five different thorax heights, as shown in Figure 8. The semi-thoracic deflection is derived from a one-dimensional element composed of impacted-side rib nodes at equivalent elevation and a thoracic cavity reference point rigidly fixed to the reinforced spinal column. The full-thoracic deflection is output by the one-dimensional discrete element established from two nodes located on the lateral aspects of the corresponding left and right ribs.

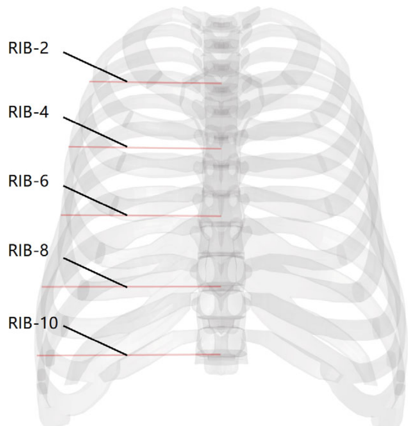

a) Semi-thoracic deflection definition and height configuration in the human model

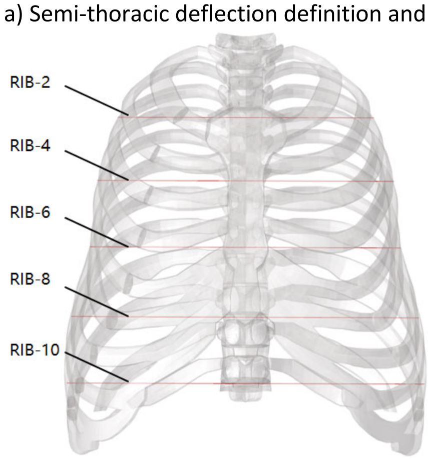

b) Full-thoracic deflection definition and height configuration in the human model

Fig. 8. Semi-thoracic deflection definition and height configuration in the human model.

III. RESULTS

Thorax Module Lateral Impact

In the thorax module lateral impact loading condition, the time-history curves of thoracic deflection for the four models are shown in Figure 9. The deviation between the thorax impactor and WorldSID in terms of maximum thorax deflection is 1.6%, while the deviations compared to THUMS and GHBMC are 11.6% and 0.2%, respectively. The thorax impactor's deflection values fell between those of the GHBMC and THUMS human body models and closely matched the WorldSID dummy's response, demonstrating that the impactor's stiffness accurately replicates the compressive characteristics of the human thorax.

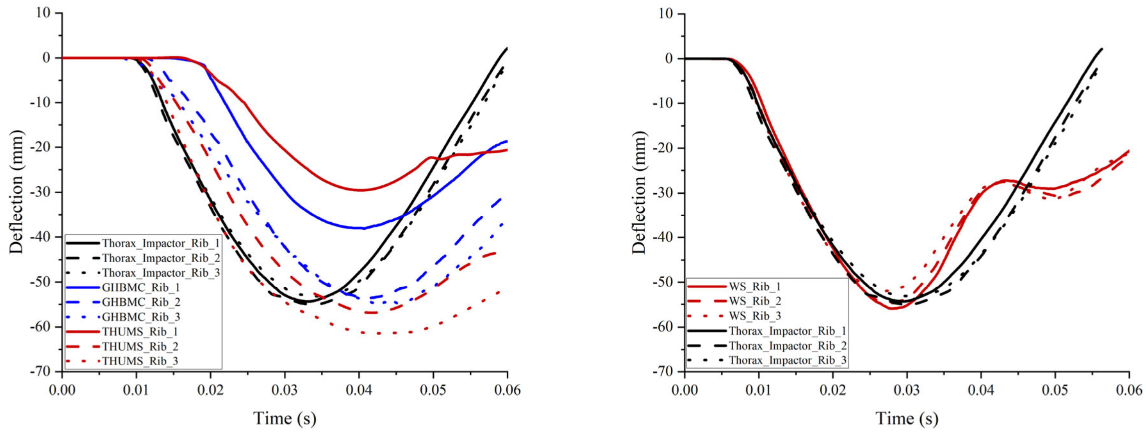

Fig. 9. Thoracic deflection responses under thorax module lateral impact loading conditions.

Full-Body Coupled Lateral Impact

The kinematic responses of the coupled thorax impactor system and the WorldSID under pendulum lateral impact loading are illustrated in Figure 10, demonstrating consistency in dynamic behaviour. Displacement and acceleration along the lateral (Y) and vertical (Z) anatomical axes at the head, T4/T8 thoracic vertebrae, and pelvic are compared in Figures A-1 and A-2, respectively. The displacement and acceleration trend remained consistent throughout the entire collision. At peak thoracic deflection (31 ms), the displacement discrepancies between models remained below 16.2%. Thus, it is evident that the thorax impactor is properly integrated with the WorldSID dummy, and the kinematic response of the thorax in the coupled model demonstrates consistency with the WorldSID. This lays the foundation for the subsequent analysis of the biofidelity of the thorax impactor.

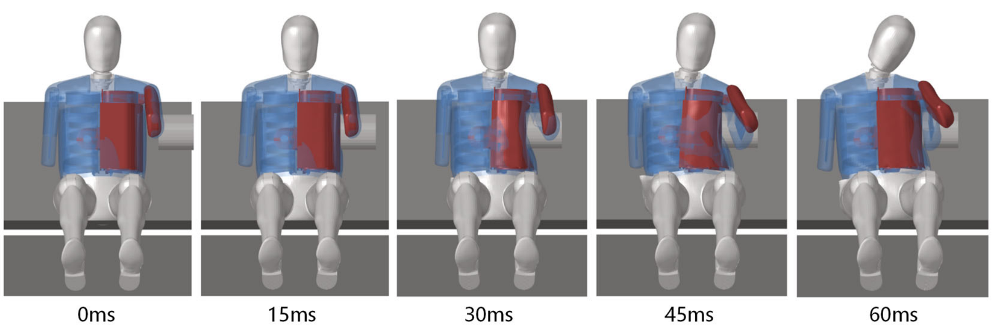

Fig. 10. Comparative kinematic analysis of coupled thorax impactor and WorldSID

Figure 11 shows the impact force time-history curve aligning with PMHS biomechanical test trends and satisfying ISO/9790 response corridor, where the thorax impactor's impact force is slightly lower than WorldSID but higher than THUMS human model.

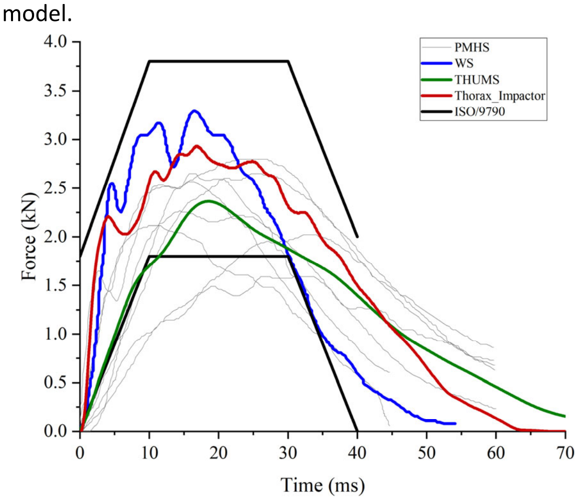

Fig. 11. Impact force-time curves of the coupled model, WorldSID and PMHS. PMHS data were obtained from [32]and [29]. The WorldSID data were taken from the dummy manual. Data of the THUMS model were derived from validation data officially released by Toyota. The pendulum mass and impact velocity were 23.4 kg and 4.3 m/s, respectively.

Thoracic Module-to-Hood Impact

In the THUMS-vehicle collision simulations, the maximum thoracic deflection for the entire thorax during the thorax-hood contact phase was extracted and compared with that of the thorax impactor under corresponding scenarios, as shown in Figure 12. This study exclusively focuses on thoracic deflection generated during thorax-vehicle contact phases. The H800A20 condition, where no thorax-hood contact occurred, has been excluded from subsequent analyses.

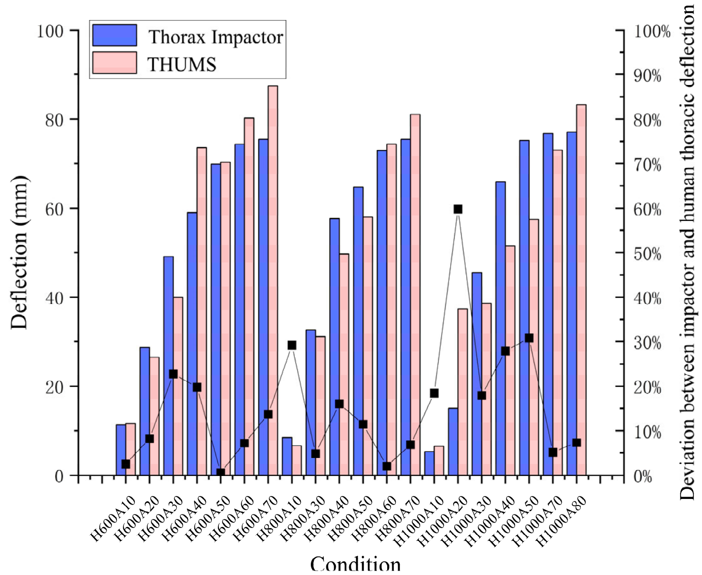

Fig. 12. Maximum thoracic deflection and deviation analysis of thorax impactor vs. THUMS in thoracic module-to-hood impact loading condition for different vehicles

Maximum thoracic deflection of the thorax impactor and THUMS were plotted in a bar chart, with differences between the two models listed as shown in Fig. 12. The results indicate that 75% of test conditions showed deviations below 20% in peak deflection, demonstrating the impactor’ s capability to predict pedestrian thoracic injuries during vehicle-pedestrian crashes.

Semi-thoracic deflections

The relationship between full-thorax (D_{full}) and semi-thoracic deflection (D_{semi}) and full-thoracic deflection (D_{full}) was established via linear fitting, as shown in Figure 13. The linear regression equation derived from the fitting is given by (R^2 = 0.568, $p < 0.05$):

$$D_{\text{semi}} = 0.391 \times D_{\text{full}} + 3.337, \tag{1}$$

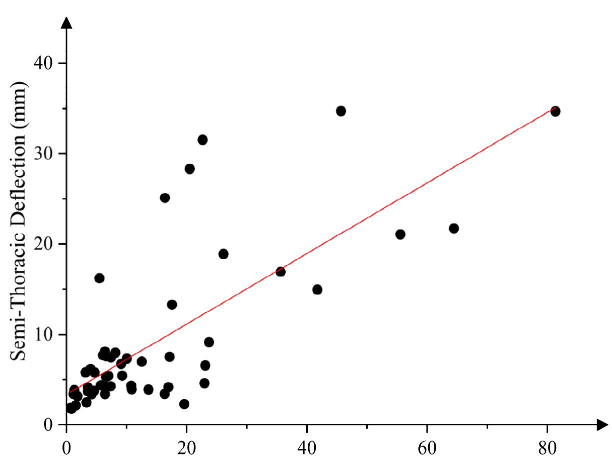

Fig. 13. Fitted curves of semi-thoracic and full-thoracic deflection in the human body.

IV. DISCUSSION

In this study, an anteroposteriorly symmetric semi-thoracic impactor with dual-bone-ring structure was designed, and performance tests under three different loading conditions were conducted to evaluate its biofidelity and deflection reproduction. Thorax Module Lateral Impact tests indicated that the peak thoracic deflection is consistent with that of the human body models. In full-body coupled lateral impact tests, the thorax impactor exhibited good deflection reproduction. In thoracic module-to-hood impact simulations, the thoracic deflection responses of the impactor and human body models showed good agreement, indicating effective deflection reproduction capability.

Figure 14 presents the impact force-deflection curves of the coupled model after converting semi-thoracic deflection to full-thoracic deflection. The response of the coupled model aligns closely with that of PMHS. During the peak deflection phase, the thorax impactor exhibits slightly larger deformation compared to PMHS, suggesting its marginally reduced stiffness in this phase. Conversely, in the initial contact phase, the thorax impactor demonstrates significantly higher stiffness than PMHS, indicating elevated contact rigidity. Given that the aggressiveness of vehicle-pedestrian impact is predominantly associated with maximum thoracic deflection, the excessive initial stiffness of the impactor may have limited influence on injury assessment outcomes.

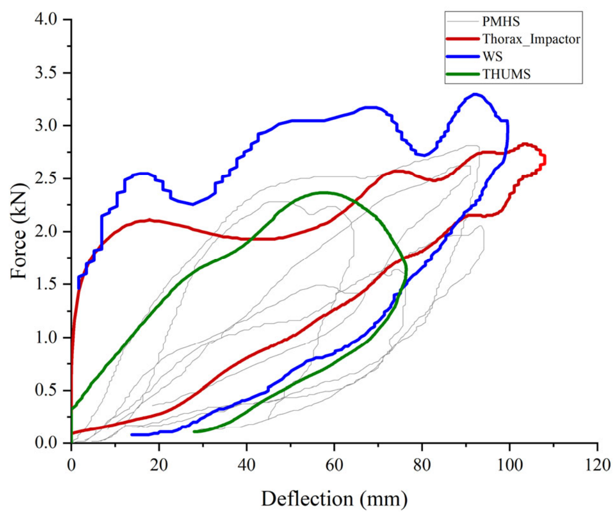

Fig. 14. Comparison of impact force-thoracic deflection curves between coupled model, dummy, and PMHS.
The data of the THUMS model were derived from validation data officially released by Toyota. The PMHS data were obtained from [29]. The pendulum mass and impact velocity were 23.4 kg and 4.3 m/s, respectively.

Figure 15 presents the deflection time-history curve converted from semi-thoracic deflection measurements of the thorax impactor. The peak deflections of the first and second thoracic ribs in the impactor fell within PMHS deflection ranges and demonstrated close agreement with WorldSID dummy data. The third thoracic rib exhibited marginally lower peak deflection, likely attributable to structural interactions between the thorax impactor and WorldSID dummy’s lumbar-abdominal junction.

Human thoracic ribs connect to the spine and sternum through articular joints, with intervertebral discs enabling relative motion between spinal vertebrae. This anatomical configuration provides natural thoracic flexibility, resulting in lower initial stiffness during lateral impact. Conversely, ATD thorax designs employ rigid mechanical connections between skeletal components to ensure testing consistency and repeatability. Such structural constraints significantly limit joint mobility between thoracic bones, consequently generating excessive initial stiffness during lateral impact simulations.

The current phase of this study focused on development and validating the thorax impactor. The relationship between its predicted thoracic deflection and pedestrian thoracic injury risk will be a key focus of future research. Statistical analyses demonstrate lower incidence rates of Rib 1 and Rib 2 injuries compared to the higher prevalence of Rib 3-7 injuries in pedestrian traffic accidents (base on China Field Accident Study System (FASS) Database). Consequently, current-phase thoracic impactor research has not prioritized the biomechanical response characterization of the superior thoracic ribs. The biomechanical influence of upper extremity kinetics on thoracic injury mechanisms presents multifaceted interdependencies that necessitate further investigation. It should be noted that the enhancement of test repeatability and reproducibility for the thoracic impactor may necessitate structural modifications with consideration of manufacturing process constraints during its fabrication.

In addition to collision speed, thoracic injury severity is closely associated with thoracic posture, as well as forces exerted by the head-neck complex and abdomen. Therefore, the injury mechanisms of pedestrian thoracic injury caused by direct vehicle impact are complex, making it difficult to replicate the chest collision (deflection) process using simple mechanical structures. Current thoracic impactor designs primarily aim to reproduce the maximum chest deflection, while the dynamic deflection process during impact serves only as a reference. Further research is still required to accurately reconstruct the dynamic deflection process of the chest during impact.

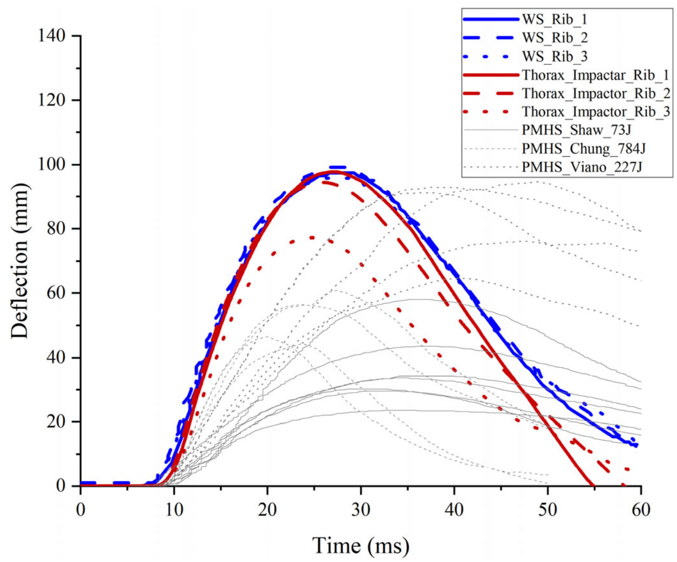

Fig. 15. Thoracic deflection-time curves of coupled models with dummy, PMHS
Human test data were obtained from [27-29].WorldSID data were taken from the dummy manual. THUMS modeling was performed using official Toyota-published validation data. The mass of the pendulum is 23.4 kg and the impact velocity is 4.3 m/s.

The parametric rationality of the impactor launching configurations (e.g., launch velocity and angular orientation) in thoracic module-vehicle collision simulations pertains fundamentally to the domain of testing evaluation methodology, warranting further systematic investigation. Establishing the injury risk correlation between thoracic deflection predicted by the impactors and pedestrian thoracic injury risk constitutes a critical research priority. Furthermore, the simplified vehicle models used in this study may exhibit performance discrepancies compared to production vehicles. Therefore, it is necessary to carry out the predictive performance analysis of the impactor in real-vehicle collisions in the future after determining the measurement method.

V. CONCLUSION

An anteroposteriorly symmetric semi-thoracic impactor with dual-bone-ring structure was developed in this study. Validation through three test conditions - thorax module lateral impact, full-body coupled lateral impact, and thoracic module-to-hood impact , demonstrated its good biofidelity and pedestrian thoracic deflection reproduction capability. The impactor shows promising applicability for future research on pedestrian thoracic injury assessment.

VI. ACKNOWLEDGEMENTS

The authors acknowledge Honda,Toyota and Cellbond for their support and help in this study.

VII. REFERENCES

[1] Lopez, A.D., Mathers, C.D., Ezzati, M., Jamison, D.T., and Murray, C.J.L. Global and regional burden of disease and risk factors, 2001: systematic analysis of population health data. *Lancet*, 2006. 367(9524): p. 1747-1757

[2] Organization, W.H., "World health statistics 2024: monitoring health for the SDGs, sustainable development goals". 2024: World Health Organization.

[3] Bahrololoom, S., Young, W., and Logan, D. Modelling injury severity of bicyclists in bicycle-car crashes at intersections. *Accident Anal Prev*, 2020. 144

[4] Strandroth, J., Sternlund, S., et al. Correlation between Euro NCAP pedestrian test results and injury severity in injury crashes with pedestrians and bicyclists in Sweden. 2014, SAE Technical Paper.

[5] Zhao, H., Yin, Z., et al. A study on adult pedestrian severe injuries and fatalities induced by passenger cars in Chongqing, China. *International Journal of Vehicle Safety*, 2015. 8(2): p. 180-191

[6] Fredriksson R., F.E., Boström O., Backman K. Injury mitigation in SUV-to-pedstrian impacts, in *20th ESV conference proceedings*. 2007. p. Paper no. 07-0308.

[7] Zander, O., Wisch, M., et al. Development and evaluation of a thorax injury prediction tool (TIPT) and possibilities for incorporation within improved test and assessment procedures–results from SENIORS. 2019

[8] Karadeniz, S.S. Design, analysis and experimental study of a novel side thorax impactor to be used in pedestrian protection tests for flat front vehicles. 2021, Middle East Technical University (Turkey).

[9] van Ratingen, M. Development and evaluation of the ES-2 side impact dummy. 2001, SAE Technical Paper.

[10] Trosseille, X. and Petitjean, A. Sensitivity of the WorldSID 50th and ES-2re Thoraces to Loading Configuration. 2010, SAE Technical Paper.

[11] Lei, L., Haitao, Z., Chong, L., and Kai, W. WorldSID 50th percentile male dummy study. *Tianjin Science and Technology*, 2014. 41(8): p. 50-54

[12] Chang, Y., Long, Y., et al. A study on the performance of WordSID thorax module for thorax injury prediction in e-Bike rider based on real accident data. *Acta of Bioengineering & Biomechanics*, 2024. 26(3)

[13] Wenle, L., Shijie, R., et al. Injury analysis of a six-year-old child pedestrian thorax in lateral/oblique impact. *Proceedings of 2016 Eighth International Conference on Measuring Technology and Mechatronics Automation (ICMTMA)*, 2016.

[14] Reddy, N.B., Madithati, P., Reddy, N.N., and Reddy, C.S. An epidemiological study on pattern of thoraco-abdominal injuries sustained in fatal road traffic accidents of Bangalore: Autopsy-based study. *Journal of emergencies, trauma, and shock*, 2014. 7(2): p. 116-120

[15] Yoganandan, N., Pintar, F.A., Gennarelli, T.A., Martin, P.G., and Ridella, S.A. Chest injuries and injury mechanisms in oblique lateral impacts. *Proceedings of 2007 International IRCOBI Conference*, 2007.

[16] Sinha, P. and Sarkar, P. Late clotted haemothorax after blunt chest trauma. *Emergency Medicine Journal*, 1998. 15(3): p. 189-191

[17] Berland, M., Oger, M., et al. Pulmonary contusion after bumper car collision: case report and review of the literature. *Respiratory medicine case reports*, 2018. 25: p. 293-295

[18] Bertrand, S., Cuny, S., et al. Traumatic rupture of thoracic aorta in real-world motor vehicle crashes. *Traffic injury prevention*, 2008. 9(2): p. 153-161

[19] Liu, W., Zhao, H., et al. Study on pedestrian thorax injury in vehicle-to-pedestrian collisions using finite element analysis. *Chinese journal of traumatology*, 2015. 18(2): p. 74-80

[20] Mirvis, S.E. Diagnostic imaging of acute thoracic injury. *Proceedings of Seminars in Ultrasound, CT and MRI*, 2004.

[21] Zhe, H. Clinical research of rib fracture and clinical anatomically measurements of ribs. 2015.

[22] McConville, J.T., "Anthropometric relationships of body and body segment moments of inertia". Vol. 32. 1981: Air Force Aerospace Medical Research Laboratory, Aerospace Medical Division ….

[23] Chandler, R., Clauser, C.E., McConville, J.T., Reynolds, H., and Young, J.W. Investigation of inertial properties of the human body. 1975.

[24] Mertz, H.J., Jarrett, K., Moss, S., Salloum, M., and Zhao, Y. The Hybrid III 10-year-old dummy. 2001, SAE Technical Paper.

[25] Standardization, C.N.I.o. Human dimensions of Chinese adults. 2023, State Administration for Market Regulation; Standardization Administration of China. p. 44.

[26] 増田光利. 衝突実験における傷害値とその測定方法. 自動車技術= Journal of Society of Automotive Engineers of Japan, 2012. 66(7): p. 24-31

[27] Chung, J., Cavanaugh, J.M., King, A.I., Koh, S.-W., and Deng, Y.-C. Thoracic injury mechanisms and biomechanical responses in lateral velocity pulse impacts. 1999, SAE Technical Paper.

[28] Shaw, J.M., Herriott, R.G., McFadden, J.D., Donnelly, B.R., and Bolte, J.H. Oblique and lateral impact response of the PMHS thorax. 2006, SAE Technical Paper.

[29] Viano, D.C. Biomechanical responses and injuries in blunt lateral impact. *SAE transactions*, 1989: p. 1690-1719

[30] Klug, C., Feist, F., et al. Development of a procedure to compare kinematics of human body models for pedestrian simulations. *Proceedings of 2017 IRCOBI conference proceedings*, 2017.

[31] Klug, C. and Ellway, J. Pedestrian human model certification. *Technical Bulletin*, 2021

[32] Eppinger, R.H., Augustyn, K., and Robbins, D.H. Development of a promising universal thoracic trauma prediction methodology. *SAE Transactions*, 1978: p. 3193-3205

VIII. APPENDIX

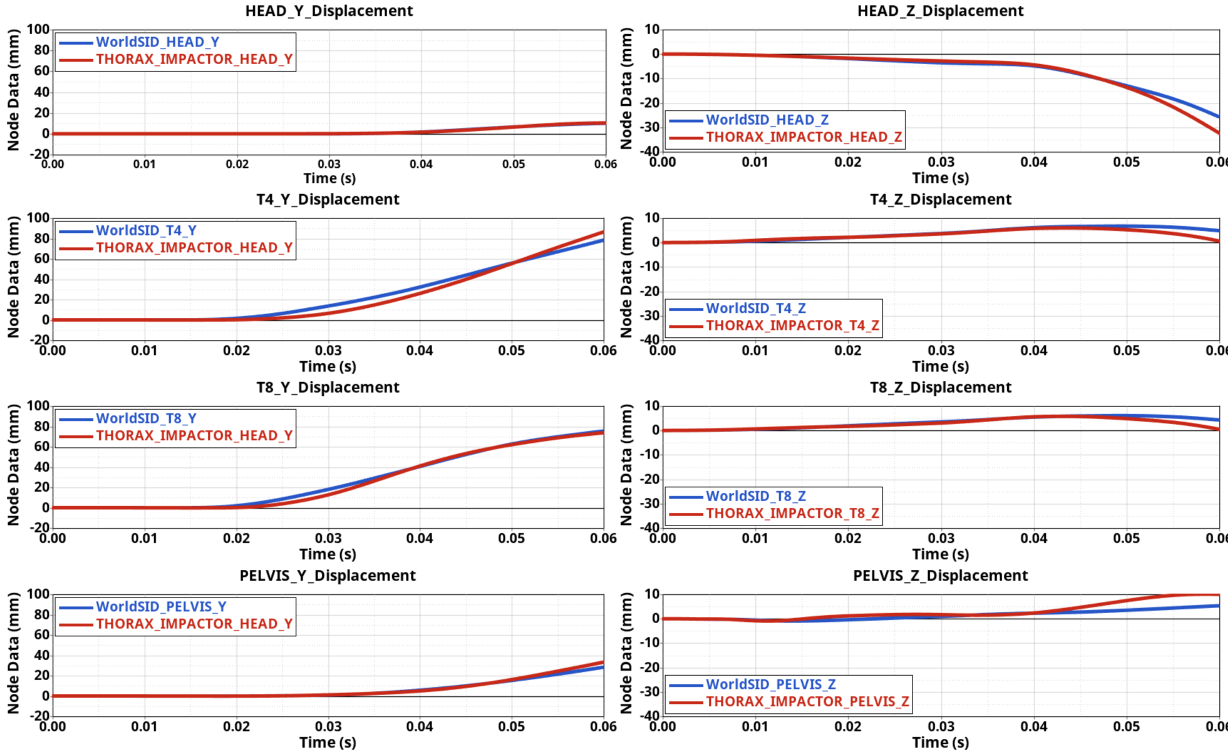

Fig. A-1. Comparison between coupled model and WorldSID displacement curve

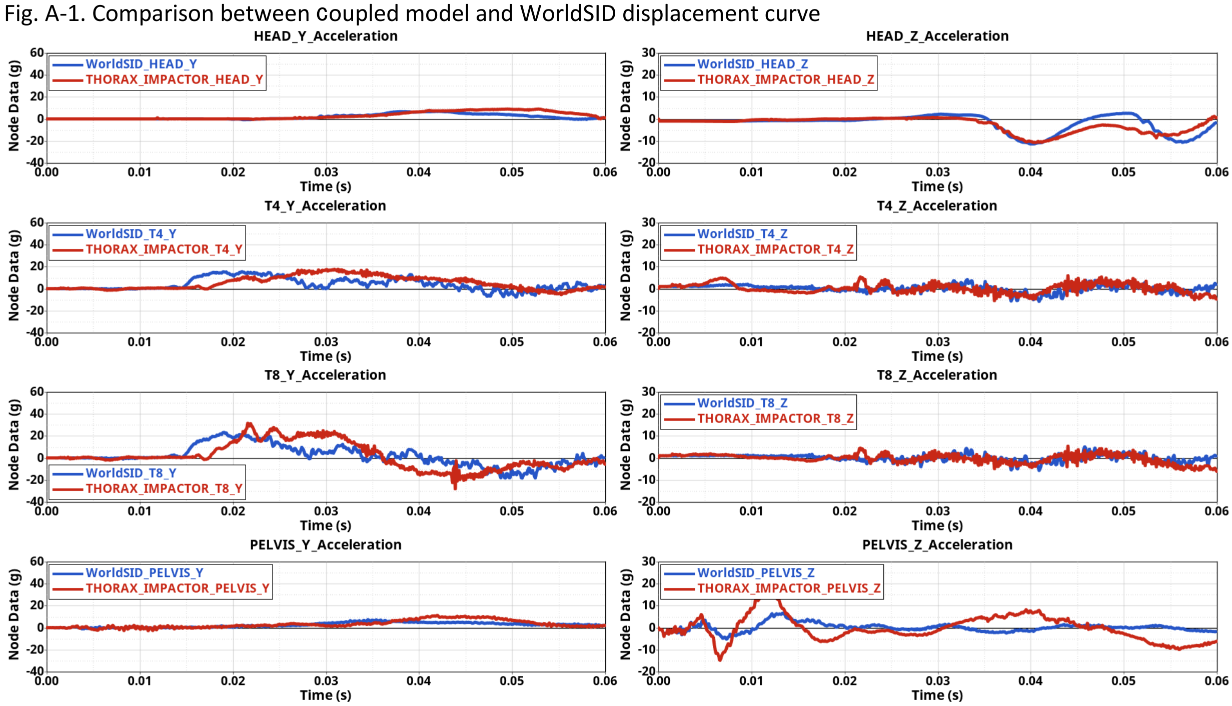

Fig. A-2. Comparison of coupled model and WorldSID acceleration curves

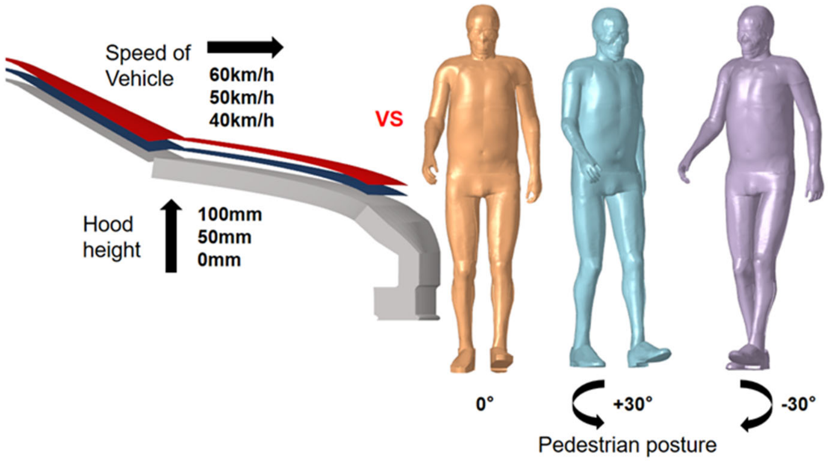

Fig. A-3 Finite element analysis of correlation between semi-thoracic and full-thoracic deflection

TABLE A-1
Maximum thoracic deflection of thorax impactor and THUMS under different operating conditions

Conditions	Velocity m/s	Shoulder Rib	Thorax Rib RIB1	Thorax Rib RIB2	Thorax Rib RIB3	Thorax Rib RIB4	THUMS Deflection
H600A10	3.80	3.36	10.53	10.65	11.05	11.31	11.6
H600A20	7.02	16.90	23.56	23.65	26.08	28.68	26.5
H600A30	8.60	25.31	34.64	38.84	44.05	49.08	40.0
H600A40	9.14	33.81	44.01	48.05	53.39	59.02	73.6
H600A50	9.92	42.25	52.67	57.43	63.18	69.86	70.3
H600A60	10.31	46.91	57.40	62.15	67.82	74.39	80.2
H600A70	10.43	47.98	58.59	63.35	69.13	75.45	87.4
H800A10	2.44	1.64	8.50	7.08	5.68	5.23	6.6
H800A30	6.84	15.11	21.78	23.71	27.71	32.60	31.1
H800A40	8.45	27.95	38.79	43.55	50.18	57.66	49.7
H800A50	9.32	36.50	47.25	51.97	57.89	64.65	58.0
H800A60	10.02	43.59	54.40	59.55	65.43	72.87	74.4
H800A70	10.43	48.23	58.91	63.83	69.45	75.46	81.0
H1000A10	1.00	0.01	5.30	3.45	3.21	3.66	6.5
H1000A20	3.82	5.43	12.13	11.75	13.64	15.03	37.4
H1000A30	6.68	18.29	27.65	31.32	38.33	45.53	38.6
H1000A40	8.15	32.65	43.85	48.83	56.77	65.88	51.5
H1000A50	9.09	41.67	53.12	58.50	66.64	75.20	57.5
H1000A70	10.44	53.34	64.76	68.98	74.00	76.75	73.0
H1000A80	10.94	54.74	66.70	71.41	74.69	77.08	83.2

TABLE A-2
THUMS simulation matrix with different vehicles, collision speeds, collision angles, and bumper heights

Number	Conditions	Collision speeds	Collision angles	Bumper heights
1	FCR－1	40km/h	+30°	0mm
2	FCR－2	40km/h	0	0mm
3	FCR－3	50km/h	+30°	0mm
4	FCR－4	50km/h	-30°	50mm
5	FCR－5	60km/h	0°	0mm
6	FCR－6	60km/h	+30°	50mm
7	SUV－1	40km/h	0	100mm
8	SUV－2	40km/h	-30°	50mm
9	SUV－3	50km/h	+30°	50mm
10	SUV－4	50km/h	-30°	100mm
11	SUV－5	60km/h	0°	100mm
12	SUV－6	60km/h	-30°	100mm